Understanding the Time Scales of the Tropospheric Circulation Response to Abrupt CO_2 Forcing in the Southern Hemisphere: Seasonality and the Role of the Stratosphere

KEVIN M. GRISE

Department of Environmental Sciences, University of Virginia, Charlottesville, Virginia

LORENZO M. POLVANI

Department of Applied Physics and Applied Mathematics, and Department of Earth and Environmental Sciences, and Lamont-Doherty Earth Observatory, Columbia University, New York, New York

(Manuscript received 25 November 2016, in final form 23 May 2017)

ABSTRACT

This study examines the time scales of the Southern Hemisphere (SH) tropospheric circulation response to increasing atmospheric CO_2 concentrations in models from phase 5 of the Coupled Model Intercomparison Project (CMIP5). In response to an abrupt quadrupling of atmospheric CO_2, the midlatitude jet stream and poleward edge of the Hadley circulation shift poleward on the time scale of the rising global-mean surface temperature during the summer and fall seasons but on a much more rapid time scale during the winter and spring seasons. The seasonally varying time scales of the SH circulation response are closely tied to the meridional temperature gradient in the upper troposphere–lower stratosphere and, in particular, to temperatures in the SH polar lower stratosphere. During summer and fall, SH polar lower-stratospheric temperatures cool on the time scale of warming global surface temperatures, as the lifting of the tropopause height with tropospheric warming is associated with cooling at lower-stratospheric levels. However, during winter and spring, SH polar lower-stratospheric temperatures cool primarily from fast time-scale radiative processes, contributing to the faster time-scale circulation response during these seasons.

The poleward edge of the SH subtropical dry zone shifts poleward on the time scale of the rising global-mean surface temperature during all seasons in response to an abrupt quadrupling of atmospheric CO_2. The dry zone edge initially follows the poleward shift in the Hadley cell edge but is then augmented by the action of eddy moisture fluxes in a warming climate. Consequently, with increasing atmospheric CO_2 concentrations, key features of the tropospheric circulation response could emerge sooner than features more closely tied to rising global temperatures.

1. Introduction

Global climate models project that, in response to increasing greenhouse gases in Earth's atmosphere, the planet's general circulation will undergo robust changes, including a poleward expansion and weakening of the Hadley circulation (Held and Soden 2006; Lu et al. 2007; Frierson et al. 2007), a poleward shift in the subtropical dry zones (Lu et al. 2007; Johanson and Fu 2009; Scheff and Frierson 2012), and a poleward shift in the midlatitude eddy-driven jet streams (Kushner et al. 2001; Barnes and Polvani 2013; Simpson et al. 2014), most notably in the Southern Hemisphere (SH). While the sign of these circulation changes is consistent across most present-day global climate models—those that participated in phase 5 of the Coupled Model Intercomparison Project (CMIP5)—there remains little consensus on the mechanisms responsible for the atmospheric circulation response (e.g., Vallis et al. 2015).

To gain better insight into the mechanisms responsible for the atmospheric circulation response to increasing greenhouse gases, a number of recent studies have begun to explore the time scales of the circulation response in global climate models. One common way to do this is to partition the circulation response into two components: 1) a fast time-scale response associated with the direct radiative forcing of increasing CO_2 and 2) a slower time-scale response associated with warming

Corresponding author: Kevin M. Grise, kmg3r@virginia.edu

DOI: 10.1175/JCLI-D-16-0849.1

sea surface temperatures (SSTs). Studies employing this methodology have concluded that the bulk of the atmospheric circulation response to increasing CO_2 arises from the warming sea surface temperatures (Stephenson and Held 1993; Deser and Phillips 2009; Staten et al. 2012; Grise and Polvani 2014a), but the direct radiative effect of the atmospheric CO_2 increase itself can also lead to rapid changes in tropical and subtropical precipitation (Bony et al. 2013; He and Soden 2017), poleward shifts of the midlatitude jets (Grise and Polvani 2014a), and changes in the strength of tropical overturning circulations (Merlis 2015; He and Soden 2015; Shaw and Voigt 2015).

Most studies on the atmospheric circulation response to increasing greenhouse gases have focused on the slower time-scale component of the response, which has been linked dynamically to warming global surface temperatures via changes in tropospheric static stability (Frierson et al. 2007; Lu et al. 2010; Kang and Lu 2012), tropopause height (Lorenz and DeWeaver 2007), upper tropospheric–lower stratospheric meridional temperature gradients (Butler et al. 2010; Arblaster et al. 2011; Wilcox et al. 2012; Harvey et al. 2014; Gerber and Son 2014), and surface meridional temperature gradients (Brayshaw et al. 2008; Ring and Plumb 2008; Butler et al. 2010; Chen et al. 2010) [see also recent review by Vallis et al. (2015)]. Relatively few studies, however, have examined the fast time-scale component of the circulation response. In the tropics, the rapid circulation response has been attributed to horizontal (Merlis 2015) and vertical (Bony et al. 2013) gradients in the direct radiative effects of CO_2, as well as to land–sea temperature contrast, which initially strengthens as landmasses warm more rapidly than oceans and promotes a fast time-scale strengthening of tropical monsoon circulations (Shaw and Voigt 2015; He and Soden 2017). In the extratropics, using a single climate model, Wu et al. (2012, 2013a) found evidence that the atmospheric circulation response initiates at stratospheric levels within the first month after an instantaneous doubling of CO_2 and then descends to tropospheric levels several months later (see also Staten et al. 2014). This initial stratospheric circulation response is driven by the direct radiative effects of CO_2 in the stratosphere, which then alters the propagation of Rossby waves in the stratosphere and upper troposphere, further changing the stratospheric winds and promoting the circulation response to couple down to tropospheric levels within a few months.

In this study, we build on these previous results and examine the time scales of the SH atmospheric circulation response to increasing atmospheric CO_2 in CMIP5 models. We focus on the SH for three reasons: 1) apart from the single-model studies of Wu et al. (2012, 2013a) and Staten et al. (2014), previous studies on the time scales of the circulation response have focused on the tropics alone, 2) the effects of land–sea temperature contrast on the circulation response are much less pronounced in the SH than in the Northern Hemisphere, thus simplifying the problem, and 3) the circulation responses in the SH extratropics are much more robust across models and straightforward to interpret. Our results provide evidence that, with increasing atmospheric CO_2 concentrations, certain key aspects of the SH atmospheric circulation response equilibrate substantially faster than the global-mean surface temperature.

2. Methodology

To conduct our analysis, we examine monthly mean output from CMIP5 global climate models (Taylor et al. 2012). CMIP5 data are freely available from the Program for Climate Model Diagnosis and Intercomparison at Lawrence Livermore National Laboratory and from the Centre for Environmental Data Analysis. Following Grise and Polvani (2016), we restrict our analysis to the 23 models with values of equilibrium climate sensitivity defined in Forster et al. (2013) (see list of models in Table 1).

For each model, we examine three different forcing scenarios: 1) preindustrial control (200+ yr runs of unforced variability), 2) abrupt $4 \times CO_2$ (150-yr runs, in which atmospheric CO_2 concentrations are abruptly quadrupled from preindustrial levels at the beginning of the run), and 3) $1\%\,yr^{-1}$ CO_2 (140-yr runs, in which atmospheric CO_2 concentrations are increased by 1% per year from preindustrial levels). For each scenario, we use one ensemble member (“r1i1p1”) per model. Following Grise and Polvani (2016), we define the preindustrial control climatology as the average of all available years of the preindustrial control run, and we estimate the $4 \times CO_2$ climatology using the average of years 101–150 from the abrupt $4 \times CO_2$ run. We exclude results from the $1\%\,yr^{-1}$ CO_2 scenario of two models (GFDL-ESM2G and GFDL-ESM2M), as they stop increasing CO_2 after 70 yr instead of 140 yr. We calculate each model’s response to CO_2 forcing as the difference between its perturbation run (abrupt $4 \times CO_2$ or $1\%\,yr^{-1}$ CO_2) and its preindustrial control climatology and then average the individual model responses together to find the multimodel-mean response.

Following Grise and Polvani (2014a), for a subset of models, we also examine three 30-yr atmosphere-only scenarios with prescribed SSTs and sea ice concentrations: 1) AMIP, 2) AMIP $4 \times CO_2$, and 3) AMIP future. These three scenarios are available from 9 of the 23

TABLE 1. Listing of the CMIP5 models used in this study. Models with AMIP, AMIP 4 × CO_2, and AMIP future runs are denoted with asterisks. (Expansions of acronyms are available online at http://www.ametsoc.org/PubsAcronymList.)

Model name	Modeling center
ACCESS1.0	Commonwealth Scientific and Industrial Research Organisation (CSIRO) and Bureau of Meteorology (Australia) (BoM)
BCC_CSM1.1*	Beijing Climate Center, China Meteorological Administration
BCC_CSM1.1(m)	Beijing Climate Center, China Meteorological Administration
CanESM2 (CanAM4*)	Canadian Centre for Climate Modelling and Analysis
CCSM4	National Center for Atmospheric Research
CNRM-CM5*	Centre National de Recherches Météorologiques/Centre Européen de Recherche et de Formation Avancée en Calcul Scientifique
CSIRO Mk3.6.0	CSIRO in collaboration with the Queensland Climate Change Centre of Excellence
FGOALS-s2	LASG, Institute of Atmospheric Physics, Chinese Academy of Sciences
GFDL CM3	National Oceanic and Atmospheric Administration (NOAA)/Geophysical Fluid Dynamics Laboratory
GFDL-ESM2G	NOAA/Geophysical Fluid Dynamics Laboratory
GFDL-ESM2M	NOAA/Geophysical Fluid Dynamics Laboratory
GISS-E2-H	National Aeronautics and Space Administration (NASA) Goddard Institute for Space Studies
GISS-E2-R	NASA Goddard Institute for Space Studies
HadGEM2-ES (HadGEM2-A*)	Met Office Hadley Centre
INM-CM4.0	Institute of Numerical Mathematics
IPSL-CM5A-LR*	L'Institut Pierre-Simon Laplace
IPSL-CM5B-LR*	L'Institut Pierre-Simon Laplace
MIROC5*	Atmosphere and Ocean Research Institute (The University of Tokyo), National Institute for Environmental Studies, and Japan Agency for Marine-Earth Science and Technology
MIROC-ESM	Japan Agency for Marine-Earth Science and Technology, Atmosphere and Ocean Research Institute (The University of Tokyo), and National Institute for Environmental Studies
MPI-ESM-LR*	Max Planck Institute for Meteorology
MPI-ESM-P	Max Planck Institute for Meteorology
MRI-CGCM3*	Meteorological Research Institute
NorESM1-M	Norwegian Climate Centre

models used in this study (see models denoted by asterisks in Table 1). The AMIP scenario uses historical radiative forcings and prescribes observed time-varying SSTs and sea ice from the 1979–2008 period. The AMIP 4 × CO_2 scenario uses the same SSTs and sea ice as the AMIP scenario but quadruples atmospheric CO_2 concentrations. The AMIP future scenario uses the same radiative forcings and sea ice as the AMIP scenario but augments the AMIP SSTs with a patterned SST anomaly based on the CMIP3 multimodel-mean SST response to 4 × CO_2 (see http://cfmip.metoffice.com/CMIP5.html for further details).

Using these scenarios, we estimate the direct radiative contribution of quadrupling atmospheric CO_2 using the difference in the climatologies of the AMIP 4 × CO_2 and AMIP runs, and we estimate the indirect (SST warming) contribution of quadrupling atmospheric CO_2 using the difference in the climatologies of the AMIP future and AMIP runs. However, we note that, in CMIP5 models, these direct and indirect contributions of 4 × CO_2 forcing are not strictly additive to the total response. The total response to 4 × CO_2 forcing (as measured by the difference of the preindustrial and abrupt 4 × CO_2 scenarios) is calculated by quadrupling CO_2 from preindustrial levels (~285 ppm), whereas the direct radiative component of the 4 × CO_2 forcing is calculated by quadrupling CO_2 from historical levels (~360 ppm). Furthermore, to calculate the indirect (SST) component of the 4 × CO_2 forcing, the SST warming pattern applied to all models is the same and is normalized to a 4-K global-mean value, whereas the SSTs for the total response (from the abrupt 4 × CO_2 scenario) vary widely according to model climate sensitivity and, in the multimodel mean, only result in a ~3.4-K global-mean value. Sea ice concentration changes are also not included in either the direct or indirect components of the response. Further discussion of this methodology is provided in Grise and Polvani (2014a) (see also Deser and Phillips 2009).

Following Grise and Polvani (2016), we utilize three metrics of the SH zonal mean atmospheric circulation (see their Fig. 1):

1) Latitude of the midlatitude eddy-driven jet (ϕ_{u850}): latitude of the maximum value of zonal mean zonal wind at 850 hPa
2) Poleward edge of the subtropical dry zone ($\phi_{P-E=0}$): latitude where the zonal mean precipitation minus

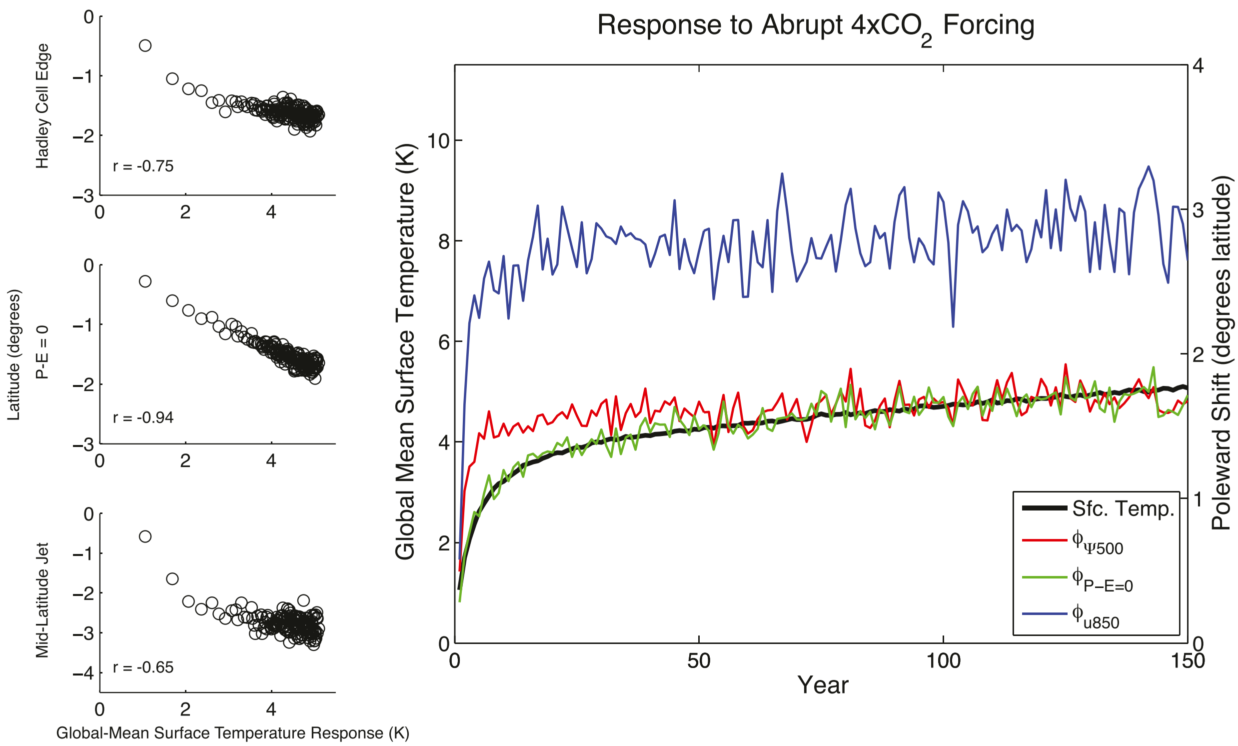

FIG. 1. (left) Scatterplots of annual-mean, multimodel-mean responses of SH (top) $\phi_{\Psi 500}$, (middle) $\phi_{P-E=0}$, and (bottom) ϕ_{u850} to abrupt $4 \times CO_2$ forcing with the coinciding global-mean surface temperature response. Each circle represents 1 yr of the 150-yr abrupt $4 \times CO_2$ scenario. (right) Time series of the annual-mean, multimodel-mean responses of global-mean surface temperature (black, K), SH $\phi_{\Psi 500}$ (red), $\phi_{P-E=0}$ (green), and ϕ_{u850} (blue) to abrupt $4 \times CO_2$ forcing.

evaporation changes sign between net evaporation in the subtropics and net precipitation at midlatitudes

3) Poleward boundary of the Hadley circulation ($\phi_{\Psi 500}$): latitude where the 500-hPa mean meridional mass streamfunction changes sign between the thermally direct overturning circulation in the tropics and the thermally indirect overturning circulation at midlatitudes

To calculate these metrics, a first guess of the latitude of each metric is estimated using the nearest latitude gridpoint i in each model. A quadratic (for ϕ_{u850}) or linear (for $\phi_{P-E=0}$ and $\phi_{\Psi 500}$) function is then fit to the three latitude grid points ($i-1$, i, and $i+1$) surrounding this first-guess estimate, and the function is used to refine the value of the metric to 0.01° latitude resolution.

3. Results

To begin, we show in Fig. 1 the annual-mean, CMIP5 multimodel-mean response of the three SH circulation metrics defined above to an abrupt quadrupling of atmospheric CO_2, together with the evolution of the global-mean surface temperature. Examining the circulation response to an abrupt change in CO_2 is useful because, in more realistic scenarios where CO_2 concentrations are increased more slowly, it is more difficult to untangle and distinguish the varying time scales of the circulation response. Figure 1 shows that the annual-mean response of SH $\phi_{P-E=0}$ to an abrupt quadrupling of CO_2 closely follows that of the global-mean surface temperature (cf. green and black lines in Fig. 1; see also scatterplot at left of Fig. 1). In contrast, the annual-mean responses of SH ϕ_{u850} and $\phi_{\Psi 500}$ do not follow the global-mean surface temperature curve. Instead, the SH midlatitude jet and Hadley cell edge initially shift poleward at a greater rate than the global-mean surface temperature warms. Specifically, 90% of the poleward shift in ϕ_{u850} and $\phi_{\Psi 500}$ occurs in the first 7 yr of the response. By comparison, 90% of the poleward shift in $\phi_{P\text{-}E=0}$ occurs after 39 yr, and 90% of the final (year-101–150 average) global-mean surface temperature response occurs after 65 yr.

The varying time scales of the circulation response shown in Fig. 1 not only are a characteristic of the multimodel mean but also occur in all individual CMIP5 models examined in this study. Figure 2 reproduces the results from Fig. 1 but shows the spread across all individual model responses. Here, to better visualize the time

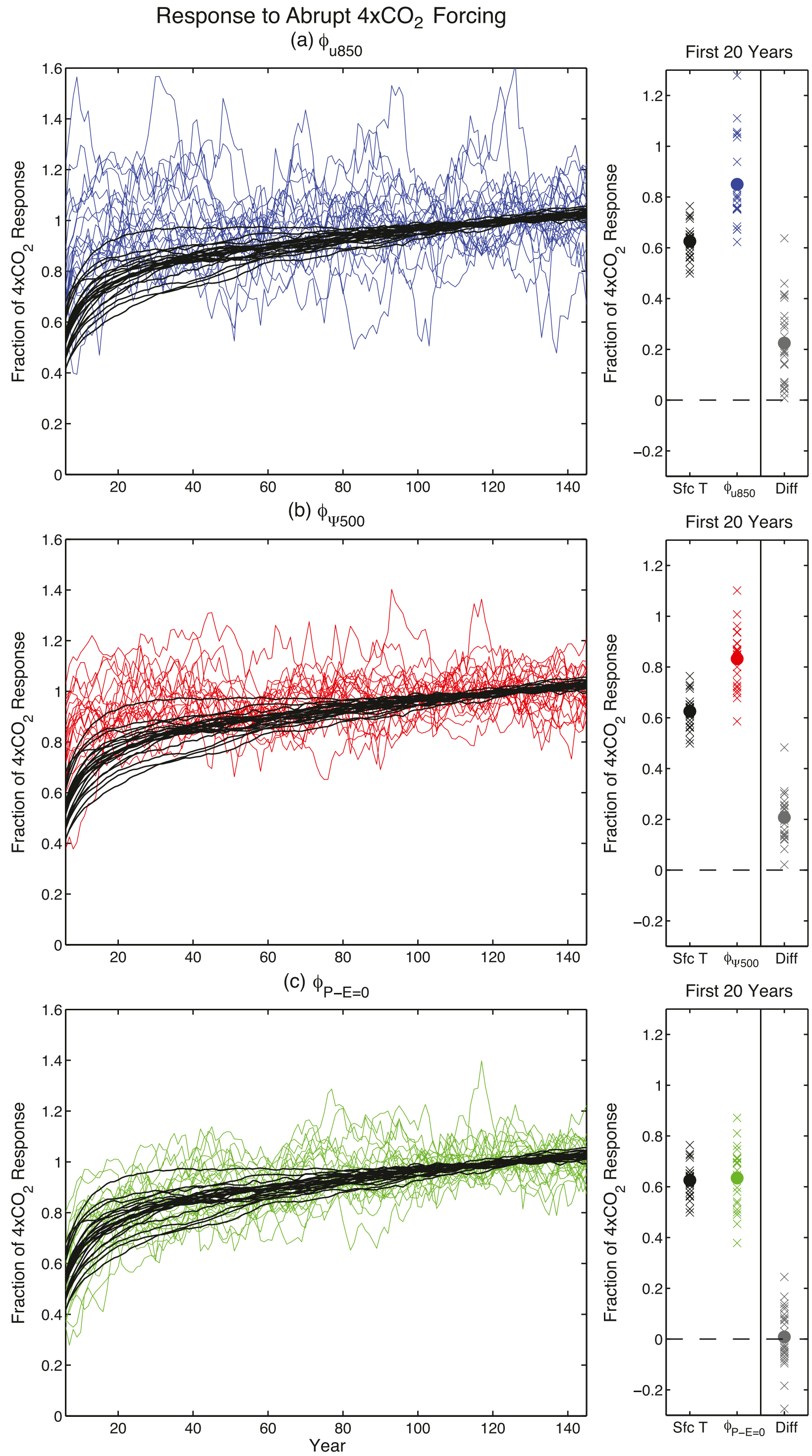

FIG. 2. (left) Time series of individual CMIP5 model annual-mean responses of SH (a) ϕ_{u850}, (b) $\phi_{\Psi500}$, and (c) $\phi_{P-E=0}$ to abrupt $4 \times CO_2$ forcing with the coinciding global-mean surface temperature responses (black lines in each panel). Individual model time series have been smoothed with an 11-yr running mean for plotting purposes. The responses are plotted in terms of the fraction of the total response to $4 \times CO_2$ (defined as the average over years 101–150). (right) Average of the responses over the first 20 yr of the abrupt $4 \times CO_2$ scenario in each model (denoted by $\times$) and the multimodel mean (denoted by •). The difference column shows the difference between the fractional response of each metric in each model and the fractional response of the global-mean surface temperature in that model.

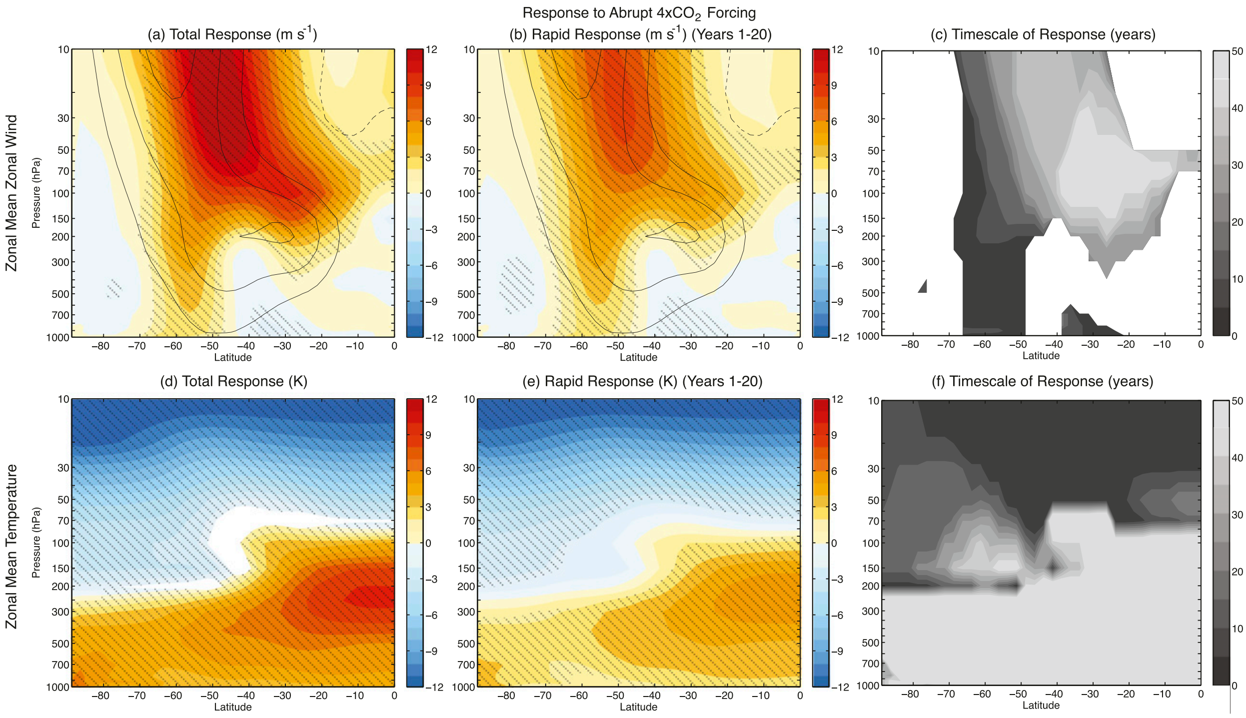

FIG. 3. Annual-mean, multimodel-mean response of (a)–(c) zonal-mean zonal wind ($m\,s^{-1}$) and (d)–(f) zonal-mean temperature (K) to $4 \times CO_2$ forcing: (a),(d) response averaged over years 101–150 of the abrupt $4 \times CO_2$ run, (b),(e) response averaged over years 1–20 of the abrupt $4 \times CO_2$ run, and (c),(f) number of years after which the response to abrupt $4 \times CO_2$ forcing reaches 90% of its final value [as shown in panels (a) and (d)]. Stippling indicates where the response is 95% statistically significant via Student's t test. Black contours in (a) and (b) show the preindustrial control climatology (contour interval: $10\,m\,s^{-1}$; solid: positive; dashed: negative; zero contour: not shown). Values in (c) are plotted only for the significant values in (a).

scales of the circulation response in each model, we plot each of the model responses in terms of the fraction of its final (year-101–150 average) response. Although these circulation metrics have large interannual variability, it is clear that, during the first ~40–60 yr of the abrupt $4 \times CO_2$ scenario, the intermodel spread in the ϕ_{u850} responses (Fig. 2a, blue lines) and $\phi_{\Psi500}$ responses (Fig. 2b, red lines) lies above the intermodel spread in the global-mean surface temperature responses (Fig. 2, black lines), whereas the intermodel spread in the $\phi_{P-E=0}$ responses (Fig. 2c, green lines) falls around the intermodel spread in the global-mean surface temperature responses. This behavior is particularly striking during the first 20 yr after CO_2 quadrupling (Fig. 2, right panels). In fact, in every single model, ϕ_{u850} and $\phi_{\Psi500}$ are adjusting to their final values on a faster time scale than the global-mean surface temperature (see difference column in Fig. 2, right). Hence, the behavior shown in Fig. 1 is pervasive across CMIP5 models.

The results in Figs. 1 and 2 raise a number of questions:

1) Why do some features of the SH tropospheric circulation (ϕ_{u850} and $\phi_{\Psi500}$) respond faster to CO_2 forcing than the global-mean surface temperature?
2) Do SH ϕ_{u850} and SH $\phi_{\Psi500}$ respond faster than the global-mean surface temperature during all seasons or only during certain seasons?
3) Why is the response of SH $\phi_{P-E=0}$ to CO_2 forcing delayed compared to that of SH ϕ_{u850} and SH $\phi_{\Psi500}$?
4) Are the results shown in Figs. 1 and 2 relevant for more realistic scenarios in which atmospheric CO_2 concentrations increase slowly over time?

We address each of these questions individually in the following four subsections.

a. Fast time-scale response of the SH tropospheric circulation

In this subsection, we address why the responses of SH ϕ_{u850} and $\phi_{\Psi500}$ to abrupt $4 \times CO_2$ forcing are faster than that of the global-mean surface temperature. For brevity, we focus on the results for SH ϕ_{u850} but note that the results for SH $\phi_{\Psi500}$ yield very similar conclusions.

First, in Fig. 3a, we review the annual-mean, multimodel-mean response of the SH zonal mean zonal wind to $4 \times CO_2$ forcing (as averaged over years 101–150 of the abrupt $4 \times CO_2$ scenario). As documented in many previous studies, the response is characterized by a

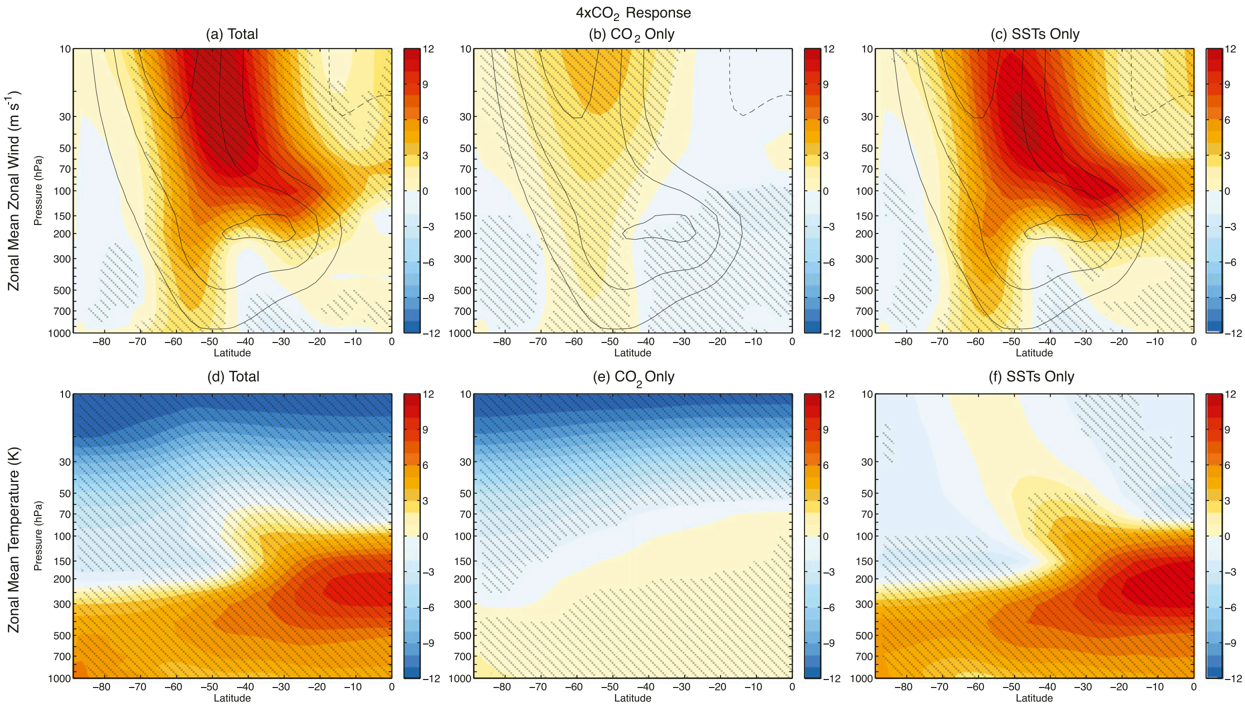

FIG. 4. As in the left column of Fig. 3, but for (a),(d) the total response to 4 × CO_2 forcing (years 101–150 of abrupt 4 × CO_2 scenario − piControl), (b),(e) the contribution from atmospheric CO_2 forcing alone (AMIP 4 × CO_2 − AMIP), and (c),(f) the contribution from increasing SSTs alone (AMIP future − AMIP). Results are shown for the nine models with AMIP, AMIP 4 × CO_2, and AMIP future runs (see Table 1). Stippling indicates regions where eight or more models agree on the sign of the response.

poleward shift in the tropospheric midlatitude westerly jet and a strengthening of winds in the subtropical and midlatitude stratosphere (e.g., Fig. 12.19 of Collins et al. 2014). However, Fig. 3b reveals that much of this response is established within the first 20 yr after an abrupt quadrupling of atmospheric CO_2, which we refer to hereafter as the "rapid response."

The rapid responses of the zonal wind in the troposphere and polar stratosphere (poleward of 60°S) appear nearly identical to their final responses (cf. Fig. 3b with Fig. 3a), even though the global-mean surface temperature response is only, on average, 63% of its final value during this period (Fig. 2, right). As further evidence of this, in Fig. 3c, we plot the number of years required for the zonal mean zonal wind response to reach 90% of its final value following an abrupt quadrupling of atmospheric CO_2. The majority of the tropospheric circulation response occurs very rapidly (within ~5 yr after CO_2 quadrupling), but note also that the circulation response at the poleward flank of the stratospheric jet occurs equally as fast. By contrast, the stratospheric wind response on the equatorward side of the stratospheric jet evolves on a much slower time scale (~30+ yr), more consistent with that of $\phi_{P-E=0}$ and the global-mean surface temperature (Fig. 1).

To understand the varying time scales of the zonal mean zonal wind response, we partition the response into two components: 1) a component due to the direct radiative forcing of 4 × CO_2 and 2) a component due to the associated warming SSTs. The results are shown in the top row of Fig. 4. Recall that the model runs necessary for this decomposition are only available for 9 models used in this study (see Table 1), but fortunately, this subset of models is able to well capture the multimodel-mean zonal mean zonal wind response (cf. Fig. 4a to Fig. 3a). The results in Fig. 4 reveal that the bulk of the zonal mean zonal wind response to 4 × CO_2 forcing can be explained through the effects of increasing SSTs alone (Fig. 4c) but that the direct radiative forcing of increasing atmospheric CO_2 is sufficient to alter the strength and position of the extratropical stratospheric jet and to shift the tropospheric jet poleward (Fig. 4b; see also Grise and Polvani 2014a). It is unlikely to be a coincidence that the features of the zonal mean zonal wind response with the fastest time scales (Fig. 3c) are the same features most impacted by the direct radiative forcing of CO_2 (Fig. 4b), suggesting that radiative processes help to initiate the faster circulation responses in these regions.

In the bottom row of Figs. 3 and 4, we repeat the analysis from the top row of Figs. 3 and 4 but for zonal

TABLE 2. Correlations between the poleward shift of SH ϕ_{u850} in response to 4 × CO_2 forcing and various temperature responses to 4 × CO_2 forcing in CMIP5 models. The responses to 4 × CO_2 forcing are calculated using averages over years 101–150 of the abrupt 4 × CO_2 scenario. Bold values indicate correlation coefficients that are statistically significant at the 95% confidence level.

	Annual	DJF	MAM	JJA	SON
Tropical upper-tropospheric temperature response (150–200 hPa; 0°–30°S)	**0.56**	**0.57**	**0.66**	0.26	0.28
Polar lower-stratospheric temperature response (150–200 hPa; 65°–90°S)	**−0.63**	**−0.54**	**−0.64**	**−0.55**	**−0.45**
Global-mean surface temperature response	0.39	**0.46**	**0.52**	0.14	0.12

mean temperature. The results reveal that temperatures at stratospheric levels rapidly equilibrate to the radiative forcing of increased CO_2, whereas temperatures at tropospheric levels evolve on the much slower time scale of the global-mean surface temperature, consistent with the warming of the global oceans (cf. Fig. 3e with Fig. 3d, and Fig. 4f with Fig. 4e). Consequently, the fast time scale of the tropospheric circulation response (as shown in Fig. 1 and Fig. 3, top row) is suggestive of driving by temperatures at stratospheric levels rather than those at tropospheric levels (cf. Fig. 3c with Fig. 3f).

The fast time-scale effects of the direct radiative forcing of CO_2 and the slower time-scale effects of increasing global surface temperatures both act to shift the tropospheric circulation poleward (Figs. 4b,c), but there is little commonality between their zonal mean temperature responses (Figs. 4e,f). Interestingly, one common feature is a cooling of the lowermost stratosphere. Previous studies have emphasized the importance of the upper troposphere–lower stratosphere meridional temperature gradient in governing the tropospheric circulation response to anthropogenic forcing (Lorenz and DeWeaver 2007; Butler et al. 2010; Arblaster et al. 2011; Wang et al. 2012; Wilcox et al. 2012; Gerber and Son 2014). Consistent with these previous studies, we find that CMIP5 models with greater tropical upper-tropospheric warming (150–200 hPa; 0°–30°S) and/or greater polar lower-stratospheric cooling (150–200 hPa; 65°–90°S) in response to 4 × CO_2 forcing (as averaged over years 101–150 of the abrupt 4 × CO_2 scenario) exhibit greater poleward shifts in the annual mean position of SH ϕ_{u850} (see correlation values listed in Table 2). Similar results can be derived for the annual mean positions of SH $\phi_{\Psi500}$ and $\phi_{P-E=0}$ (not shown). However, in the case of SH ϕ_{u850}, only the correlations with the polar lower-stratospheric cooling response are significant during all four seasons (Table 2), a point to which we will return in the next subsection.

To summarize, large facets of the tropospheric circulation response to abrupt 4 × CO_2 forcing evolve within the first 20 yr, even though, on average, only 63% of global surface temperature warming has occurred during this period (Fig. 2, right). Although the majority of the tropospheric circulation response can be attributed to rising global surface temperatures (Fig. 4c), the features of the tropospheric circulation that respond the fastest to abrupt CO_2 forcing are very similar to those driven by the direct radiative effects of CO_2 (cf. Fig. 3b with Fig. 4b). The meridional temperature gradient in the upper troposphere–lower stratosphere (which can be affected by both radiative processes and SST warming) appears to be key in explaining the intermodel variance of the tropospheric circulation response (Table 2). These linkages among the tropospheric circulation response, radiative processes, global surface temperature warming, and upper troposphere–lower stratosphere temperatures are explored further in the next subsection, where we examine the seasonality of the responses.

b. *Seasonality*

In this subsection, we address the seasonality of the SH tropospheric circulation response to abrupt 4 × CO_2 forcing. It is important to note that the abrupt 4 × CO_2 scenario in CMIP5 models is initialized at the beginning of the calendar year, so we caution readers from focusing on the seasonality of the first year of the response, as it depends on the time of year when the forcing is imposed (see Wu et al. 2013a).

In Fig. 5, we show the responses of SH ϕ_{u850}, $\phi_{\Psi500}$, and $\phi_{P-E=0}$ to abrupt 4 × CO_2 forcing for all four seasons: December–February (DJF), March–May (MAM), June–August (JJA), and September–October (SON). Consistent with Fig. 1, the poleward shift of $\phi_{P-E=0}$ closely follows the global-mean surface temperature response during all four seasons (Fig. 5c). In contrast, the rapid responses of ϕ_{u850} and $\phi_{\Psi500}$ to abrupt 4 × CO_2 forcing (Fig. 1, blue and red lines) appear to arise primarily from JJA and SON; during DJF and MAM, the responses of ϕ_{u850} and $\phi_{\Psi500}$ instead more closely follow the global-mean surface temperature response (Figs. 5a,b). The seasonality of the circulation responses can be better visualized by examining averages over the first 20 yr after CO_2 quadrupling (Fig. 5, right). SH ϕ_{u850} adjusts to its final value on a faster time scale during JJASON in all but one model (Fig. 5a, right), and SH $\phi_{\Psi500}$ adjusts to its final value on a faster time scale during JJASON in all but three models (Fig. 5b, right). In contrast, only 65% of models (15 out of 23) show SH $\phi_{P-E=0}$ adjusting to its final value on a faster time scale during JJASON (Fig. 5c, right).

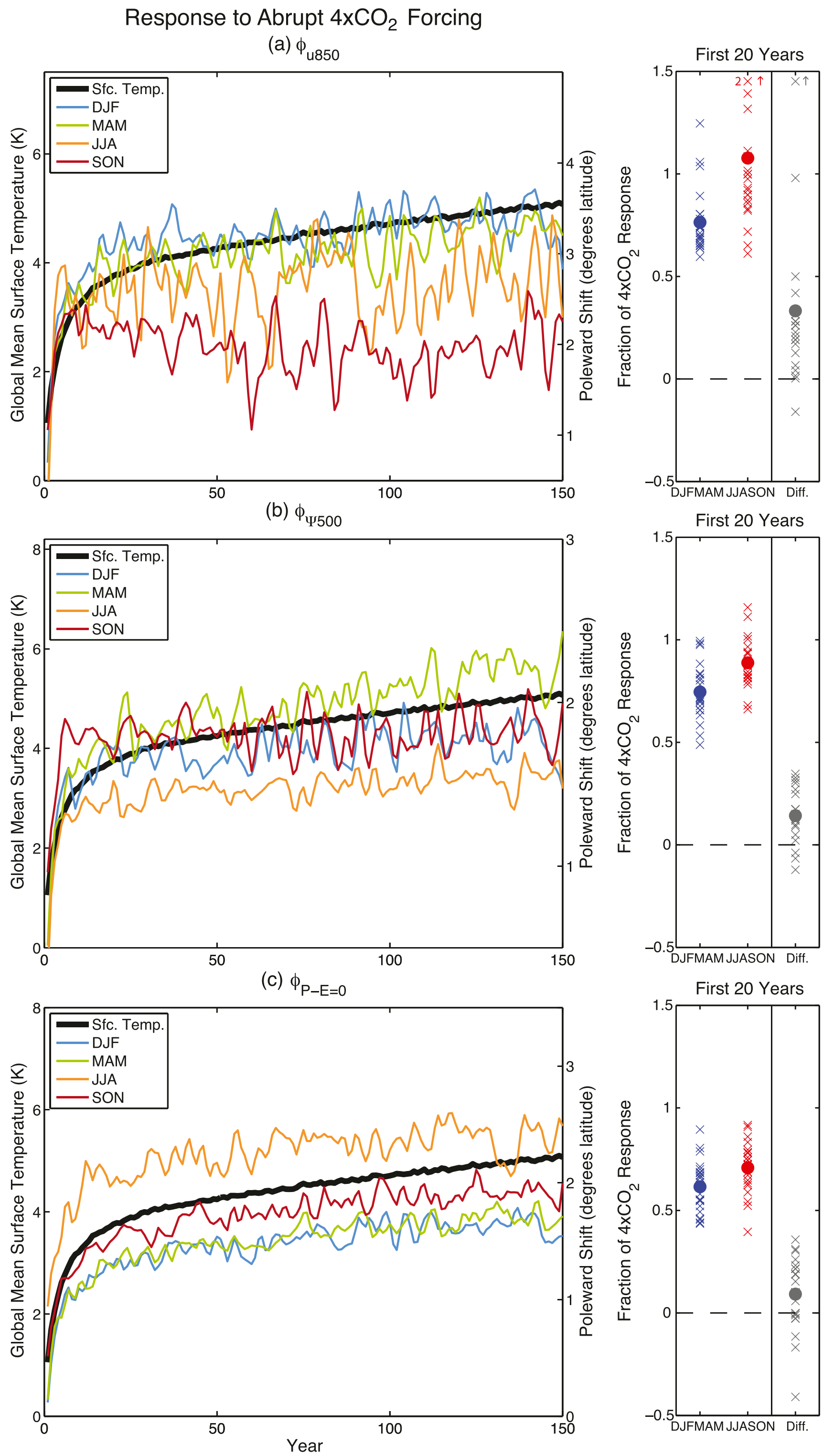

FIG. 5. (left) Seasonal-mean multimodel-mean responses to abrupt 4 × CO_2 forcing: (a) SH ϕ_{u850}, (b) SH $\phi_{\Psi500}$, and (c) SH $\phi_{P-E=0}$. The annual-mean, multimodel-mean, global-mean surface temperature response is the black line in each panel. The time series have been low-pass filtered for plotting purposes. (right) As in the right column of Fig. 2, but for averages over the first 20 yr of the abrupt 4 × CO_2 scenario in each model for the DJFMAM and JJASON seasons; the small upward-pointing red and gray arrows at the top of the top panel indicate outliers lying outside the axes bounds. Fractional responses are only plotted for those models whose final responses exceed 0.5° latitude.

Based on the correlations in Table 2, one might speculate that the seasonality in the time scales of the circulation responses shown in Fig. 5 reflects seasonality in the time scales of temperatures in the upper troposphere and lower stratosphere. To explore this hypothesis, in Fig. 6, we show the multimodel-mean response of tropical upper-tropospheric temperatures and polar lower-stratospheric temperatures to an abrupt quadrupling of atmospheric CO_2 for all four seasons. During all seasons, the tropical upper-tropospheric temperatures evolve on the time scale of the global-mean surface temperature, consistent with the moist adiabatic adjustment of tropical tropospheric lapse rates to surface warming (Fig. 6a). In contrast, the response of polar lower-stratospheric temperatures exhibits distinct seasonality. During DJF and MAM, polar lower-stratospheric temperatures cool on a time scale similar to that of the global-mean surface temperature rise (Fig. 6b, compare blue and green lines to black line). However, during JJA and SON, polar lower-stratospheric temperatures maintain an approximately constant level of cooling (1–2 K) throughout the duration of the 150-yr run. We note that this behavior is robust across models: in all but one model, polar lower-stratospheric temperatures adjust to their final values on a faster time scale during JJASON (Fig. 6b, right).

The seasonality of the polar lower-stratospheric temperature response can be explained by the climatology of the vertical temperature profile at SH high latitudes. During summer months (DJF), temperatures increase with height above the polar tropopause owing to the effects of ozone heating (Fig. 7a). Because the temperature lapse rate changes sign at the tropopause, if the tropopause temperature remains fixed, an increase in tropopause height will, by definition, be associated with cooling at lower-stratospheric levels (Fig. 7a; Lorenz and DeWeaver 2007; see also Fig. 11 of Vallis et al. 2015). In response to abrupt $4 \times CO_2$ forcing, the tropopause height increases as tropospheric temperatures warm (Fig. 6c), so lower-stratospheric cooling associated with tropopause height increases will evolve on a time scale similar to that of the global-mean surface temperature (Fig. 6b, blue and green lines; see also longer time scales in the lower stratosphere in Fig. 3f). Evidence for this effect can also be seen by partitioning the DJF zonal mean temperature response to $4 \times CO_2$ forcing into the components associated with the direct radiative forcing of CO_2 and increasing SSTs (Fig. 8, top row). The results confirm that the majority of the polar lower-stratospheric cooling response during DJF can be attributed to the warming of surface temperatures (Fig. 8c) rather than to the direct radiative effects of increased CO_2 (Fig. 8b).

During winter months (JJA), the tropopause is nearly absent at SH high latitudes, as temperatures continually decrease with height into the stratosphere owing to the lack of ozone heating (Fig. 7b). Because there is little change in lapse rate across the tropopause, the increasing tropopause height during these seasons (Fig. 6c, orange and red lines) does not strongly project on polar lower-stratospheric temperatures (cf. red and black lines in Fig. 7b). Consequently, in contrast to DJF, the majority of the polar lower-stratospheric cooling response during JJA can be attributed to the direct radiative effects of CO_2 (Fig. 8e) rather than to warming surface temperatures (Fig. 8f). In fact, the warming of the SSTs actually contributes to a slight warming of the polar lower stratosphere during JJA and SON (Fig. 8f; see also Figs. 6b and 7b). As a result, the polar lower-stratospheric cooling response during these seasons is weaker and is dominated by the fast time-scale effects of radiative processes.

The seasonally varying time scales of the SH ϕ_{u850} and $\phi_{\Psi500}$ responses (as shown in Figs. 5a,b) are consistent with driving by the seasonally varying polar lower-stratospheric temperature responses (as shown in Fig. 6b). To provide support for this hypothesis, in Table 3, we partition the poleward shift of SH ϕ_{u850} in response to $4 \times CO_2$ forcing into the components associated with the direct radiative effects of CO_2 and increasing SSTs, keeping in mind that the two components are not required to be additive to the total response (see section 2). Consistent with Fig. 4c, the poleward shift in ϕ_{u850} is dominated by the effects of SST warming, but note that the impact of the SSTs on ϕ_{u850} is substantially smaller during JJA and SON. During these seasons, the warming of the SSTs does not contribute to cooling in the polar lower stratosphere and hence does not as strongly enhance the meridional temperature gradient in the upper troposphere–lower stratosphere (cf. Figs. 8c and 8f). Consequently, the direct radiative effects of increasing CO_2 play a greater relative role in driving the poleward shift in ϕ_{u850} during JJA and SON, consistent with the faster time scales of the polar lower-stratospheric temperature response (Fig. 6b) and ϕ_{u850} and $\phi_{\Psi500}$ responses (Figs. 5a,b) during these seasons.

The relationship between the polar lower-stratospheric temperature response and the tropospheric circulation response is also supported by examining the intermodel spread of CMIP5 models. As shown in Table 2, models with greater polar lower-stratospheric cooling in response to $4 \times CO_2$ forcing (as averaged over years 101–150 of the abrupt $4 \times CO_2$ run) exhibit greater poleward shifts in SH ϕ_{u850} during all seasons (see also Fig. 11 of Lorenz and DeWeaver 2007), whereas models with greater upper-tropospheric warming and global-mean surface temperature warming only exhibit greater poleward shifts in SH

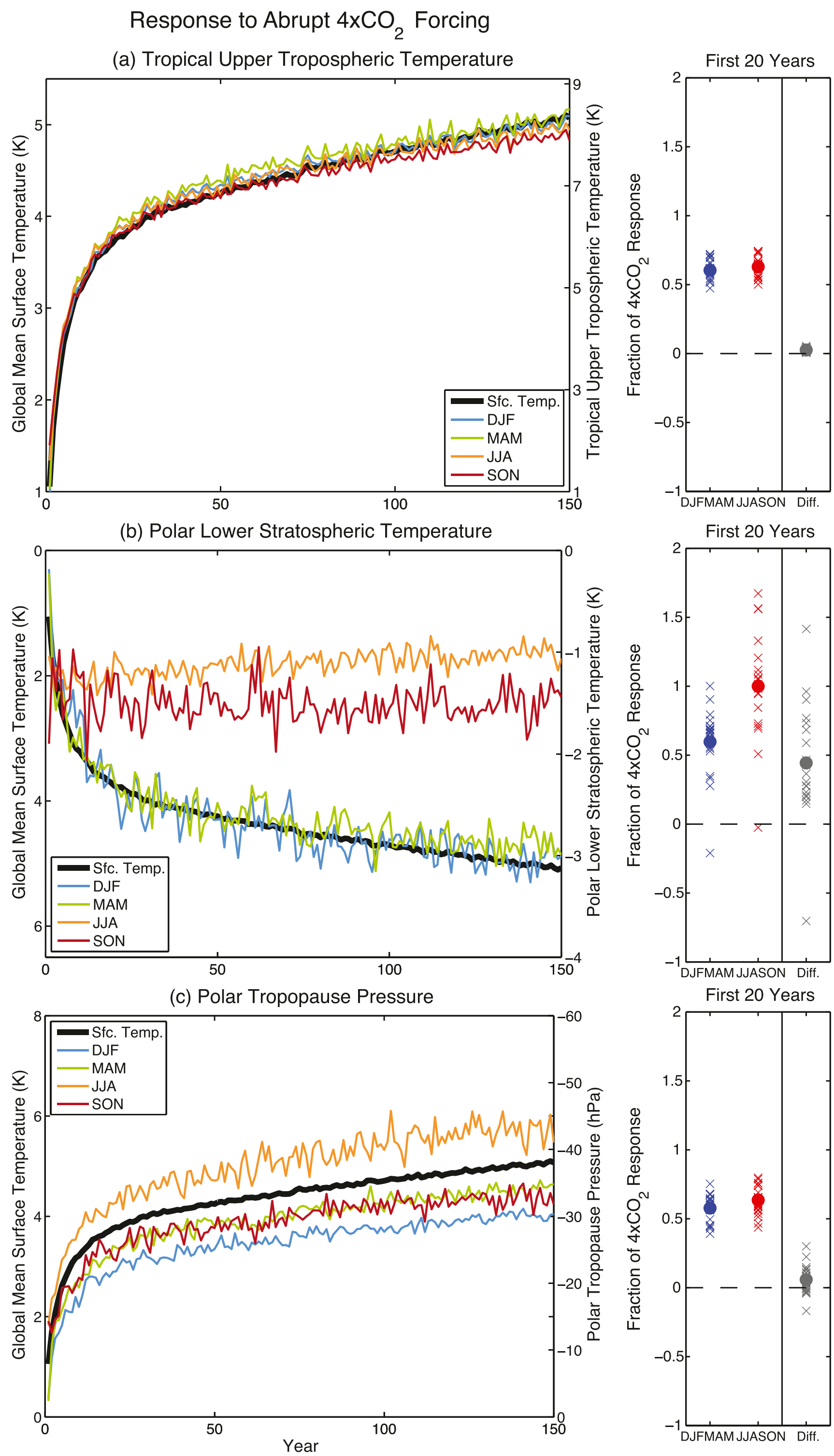

FIG. 6. As in Fig. 5, but for the responses of (a) tropical upper-tropospheric temperatures (150–200 hPa; 0°–30°S), (b) polar lower-stratospheric temperatures (150–200 hPa; 65°–90°S), and (c) polar tropopause pressure (65°–90°S) determined using the method of Reichler et al. (2003). In the left panels, the axes have been reversed for the global-mean surface temperature response in (b) and the tropopause pressure response in (c). In the right panel of (b), fractional responses are only plotted for those models whose final polar lower-stratospheric cooling responses exceed 0.5 K.

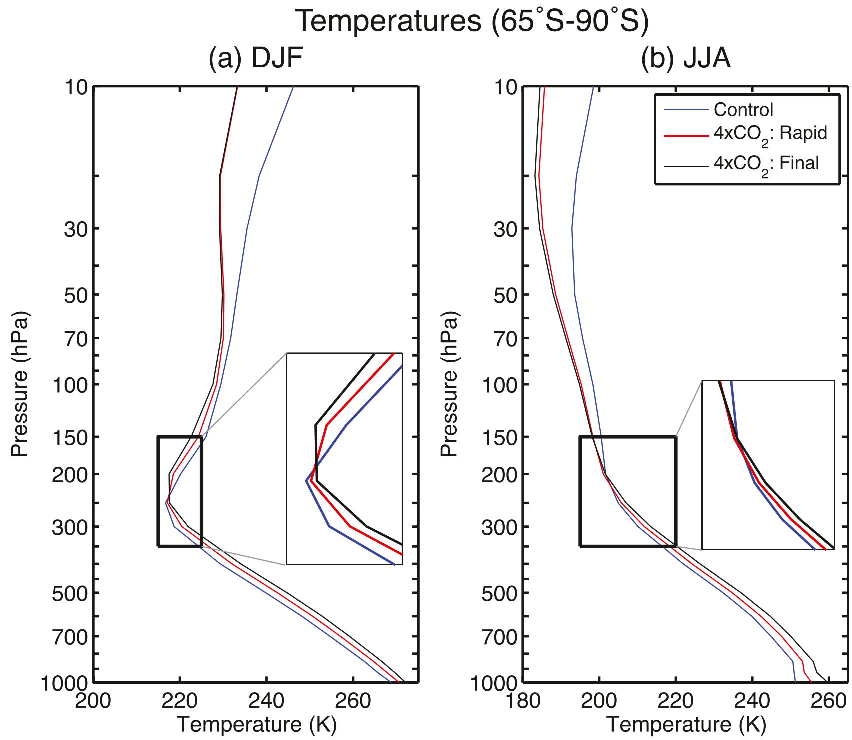

FIG. 7. Multimodel-mean vertical profiles of temperature averaged over the 65°–90°S latitude band: preindustrial control (blue), abrupt 4 × CO_2 scenario (averaged over years 1–20, red), and abrupt 4 × CO_2 scenario (averaged over years 101–150, black) for (a) DJF and (b) JJA.

ϕ_{u850} during DJF and MAM (see also Grise and Polvani 2014b, 2016). The correlations between the tropospheric circulation response and the polar lower-stratospheric temperature response during DJF and MAM are easily explained by the intermodel spread in climate sensitivity, as the polar lower-stratospheric temperature response during these seasons is largely driven by rising global surface temperatures (Figs. 7a and 8c) and thus is significantly correlated with a model's climate sensitivity ($r = -0.51$ for DJF and $r = -0.42$ for MAM). The correlations between the SH ϕ_{u850} response and the polar lower-stratospheric temperature response during JJA and SON are more surprising, given that the polar lower-stratospheric temperature response during these seasons is not significantly correlated with a model's climate sensitivity ($r = 0.17$ for JJA and $r = -0.18$ for SON). For interested readers, we provide further discussion in the appendix of the factors unrelated to climate sensitivity that may be important in governing the intermodel spread in the SH ϕ_{u850} response during JJA and SON. Finally, we note that evidence for the role of polar lower-stratospheric temperatures in the SH $\phi_{\Psi500}$ response is much less convincing than for SH ϕ_{u850}, as the intermodel spread in the SH $\phi_{\Psi500}$ response is more strongly correlated with climate sensitivity than with the polar lower-stratospheric temperature response during all seasons (see Grise and Polvani 2014b, 2016).

To summarize, in response to abrupt 4 × CO_2 forcing, we have shown that SH ϕ_{u850} and $\phi_{\Psi500}$ respond on a faster time scale than the global-mean surface temperature (Fig. 1) and that this faster time-scale response arises primarily from the JJA and SON seasons (Fig. 5). The seasonally varying time scales of the tropospheric circulation response are consistent with driving by temperatures in the polar lower stratosphere, which are more strongly influenced by fast time-scale radiative processes during JJA and SON (Figs. 6b and 8). Numerous studies have linked variability in SH polar stratospheric temperatures to variability in the SH tropospheric circulation: in the case of interannual variability during austral spring (Thompson and Wallace 2000; Thompson et al. 2005), in the case of stratospheric ozone depletion during both austral summer (Thompson and Solomon 2002; Polvani et al. 2011; Thompson et al. 2011) and austral fall (Ivy et al. 2017), and in idealized model experiments (e.g., Polvani and Kushner 2002; Williams 2006; Butler et al. 2010). Our results add to this preponderance of evidence by suggesting that polar stratospheric temperatures may also be relevant in interpreting some aspects of the tropospheric circulation

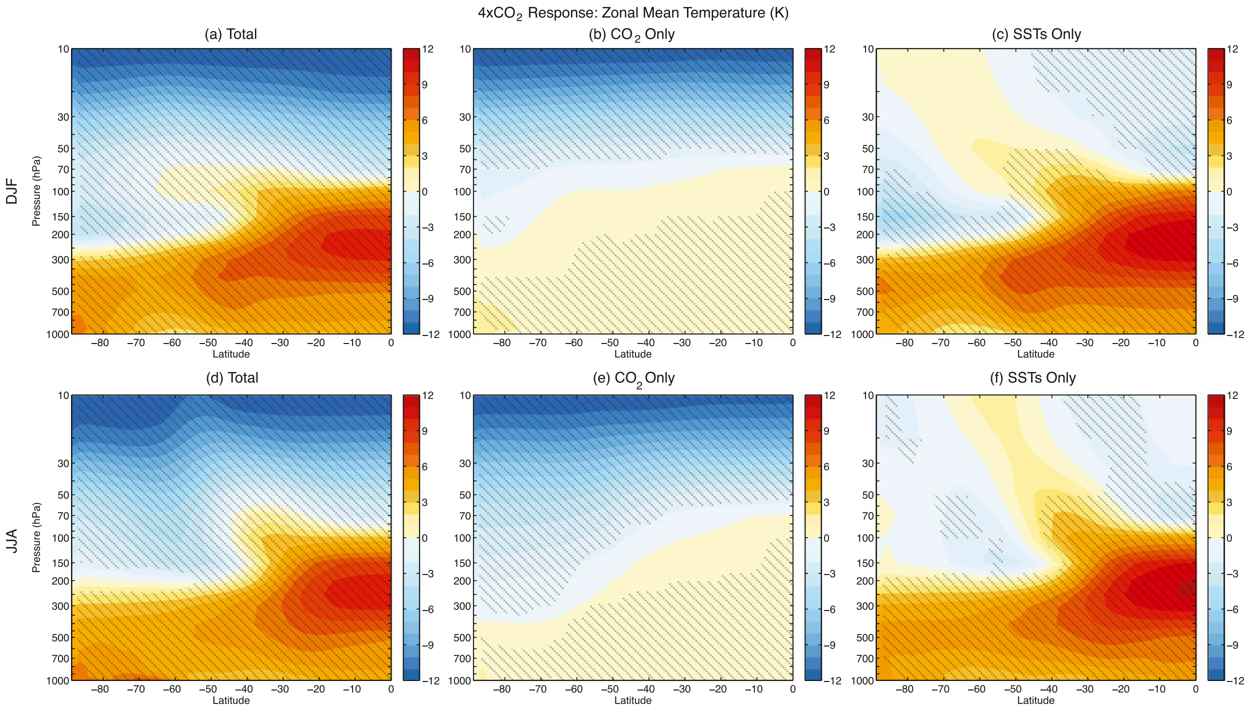

FIG. 8. As in the bottom row of Fig. 4, but for the (top) DJF and (bottom) JJA seasons.

response to CO_2 forcing [see also Wu et al. (2013a) and Staten et al. (2014)]. However, it is important to emphasize that our results here simply show correlation and not causality. The causal mechanisms linking polar stratospheric temperature variability to tropospheric circulation variability remain elusive despite over a decade of community efforts to understand them (see discussion in section 5 of Garfinkel et al. 2013).

c. *Delayed response of the SH subtropical dry zone edge*

Next, we address why the SH $\phi_{P-E=0}$ response to increasing atmospheric CO_2 appears delayed compared to the SH ϕ_{u850} and $\phi_{\Psi500}$ responses (Fig. 1). This is somewhat surprising given the strong covariability between the poleward edges of the Hadley circulation and subtropical dry zones noted in previous studies (Lu et al. 2007; Polvani et al. 2011; Kang and Polvani 2011; Quan et al. 2014; Solomon et al. 2016). To understand the SH $\phi_{P-E=0}$ response, we decompose the response of the zonal mean precipitation minus evaporation ($P - E$) field into three components, following Seager et al. (2010) and Wu et al. (2013b):

$$\delta\langle\overline{P}-\overline{E}\rangle \approx \delta(\mathrm{TH}) + \delta(\mathrm{MCD}) + \delta(\mathrm{TE}), \qquad (1)$$

$$\delta(\mathrm{TH}) = \frac{-1}{ag\rho_w}\int_0^{p_s}\frac{1}{\cos\phi}\frac{\partial}{\partial\phi}\langle\overline{v}(\delta\overline{q})\rangle\cos\phi\,dp, \qquad (2)$$

$$\delta(\mathrm{MCD}) = \frac{-1}{ag\rho_w}\int_0^{p_s}\frac{1}{\cos\phi}\frac{\partial}{\partial\phi}\langle(\delta\overline{v})\overline{q}\rangle\cos\phi\,dp, \quad \text{and} \qquad (3)$$

$$\delta(\mathrm{TE}) = \frac{-1}{ag\rho_w}\int_0^{p_s}\frac{1}{\cos\phi}\frac{\partial}{\partial\phi}\delta\langle\overline{v'q'}\rangle\cos\phi\,dp. \qquad (4)$$

In Eqs. (1)–(4), the symbols are defined as follows: angled brackets denote zonal means, overbars denote monthly means, primes denote deviations from the

TABLE 3. Multimodel-mean poleward shift of SH ϕ_{u850} in response to $4 \times CO_2$ forcing: the top row shows the total response to $4 \times CO_2$ forcing (years 101–150 of abrupt $4 \times CO_2$ scenario $-$ piControl), the middle row shows the contribution from atmospheric CO_2 forcing alone (AMIP $4 \times CO_2$ $-$ AMIP), and the bottom row shows the contribution from increasing SSTs alone (AMIP future $-$ AMIP). The 95% confidence bounds are provided. Results are shown for the nine models with AMIP, AMIP $4 \times CO_2$, and AMIP future runs (see Table 1).

	Annual	DJF	MAM	JJA	SON
Total	3.01 ± 1.27	3.41 ± 1.28	3.48 ± 1.37	3.57 ± 2.38	1.69 ± 1.57
CO_2 only	0.83 ± 0.39	0.75 ± 0.44	0.66 ± 0.22	1.16 ± 0.84	0.94 ± 0.71
SSTs only	2.81 ± 0.40	3.56 ± 0.61	3.25 ± 0.59	2.30 ± 0.62	1.67 ± 0.62

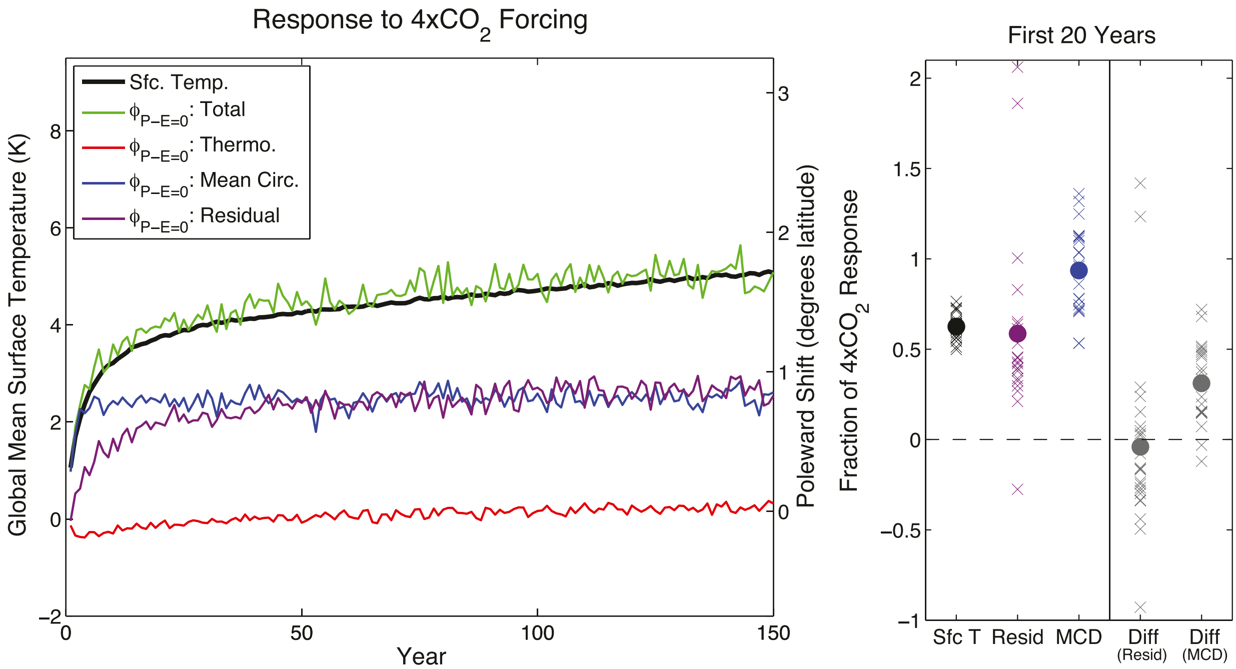

FIG. 9. (left) As in the right panel of Fig. 1, but for the decomposition of the total $\phi_{P-E=0}$ response (green) into the thermodynamic (red), mean circulation (blue), and residual (purple; total − thermodynamic − mean circulation) components defined in Eq. (1). (right) As in the right panels of Fig. 2, but for the surface temperature, residual, and MCD terms. The difference column shows the difference between the fractional response of the residual and MCD terms and the fractional response of the global-mean surface temperature in that model.

monthly mean, a is Earth's radius, g is the gravitational acceleration, ρ_w is the density of water, p_s is surface pressure, p is pressure, ϕ is latitude, v is meridional wind, and q is specific humidity. The term δ(TH) [Eq. (2)] represents changes in $P - E$ due to changes in thermodynamics (specific humidity) with the mean circulation field fixed, the term δ(MCD) [Eq. (3)] represents changes in $P - E$ due to changes in the mean circulation with the specific humidity field fixed, and the term δ(TE) [Eq. (4)] represents changes in $P - E$ due to transient eddy moisture flux convergence. Following Wu et al. (2013b), we have neglected nonlinear and surface terms in Eq. (1), which are assumed to be small (see Seager and Naik 2012).

Figure 9 shows the decomposition of the annual-mean, multimodel mean SH $\phi_{P-E=0}$ response to an abrupt quadrupling of atmospheric CO_2 (as shown in Fig. 1, green) using Eq. (1). The thermodynamic term δ(TH) does little to change $\phi_{P-E=0}$; the increases in moisture in a warmer climate simply amplify the climatological $P - E$ field in a wet-get-wetter, dry-get-drier response (e.g., Allen and Ingram 2002; Held and Soden 2006). The mean circulation term δ(MCD) leads to a rapid ~0.8° poleward shift in $\phi_{P-E=0}$ within a decade of the abrupt quadrupling of CO_2, consistent with the time scale of the responses of SH ϕ_{u850} and $\phi_{\Psi500}$ shown in Fig. 1. The mean circulation term adjusts to its final value on a faster time scale than the global-mean surface temperature in all but two models (Fig. 9, right).

The transient eddy moisture convergence term δTE cannot be directly calculated for most models, as only five models provide the necessary daily data required to calculate it. Instead, we estimate this term using the residual between the total $P - E$ response [left-hand side of Eq. (1)] and the δ(TH) and δ(MCD) terms. The resulting residual $\phi_{P-E=0}$ response (Fig. 9, purple line) evolves on a very similar time scale as the total $\phi_{P-E=0}$ response (Fig. 9, green line) and the global-mean surface temperature response (Fig. 9, black line; see also scatterplot in right panel), suggesting that eddy moisture fluxes are key to the delayed response of the subtropical dry zone edge relative to the response of the jet and Hadley cell edge. This is supported by a direct calculation of the δ(TE) term using the available models with daily data, which show that the majority (~55%) of the residual $\phi_{P-E=0}$ response (Fig. 9, purple line) can be attributed to eddy moisture fluxes (not shown). The effects of the transient eddy moisture flux convergence on SH $\phi_{P-E=0}$ increase throughout the duration of the abrupt $4 \times CO_2$ scenario as specific humidity

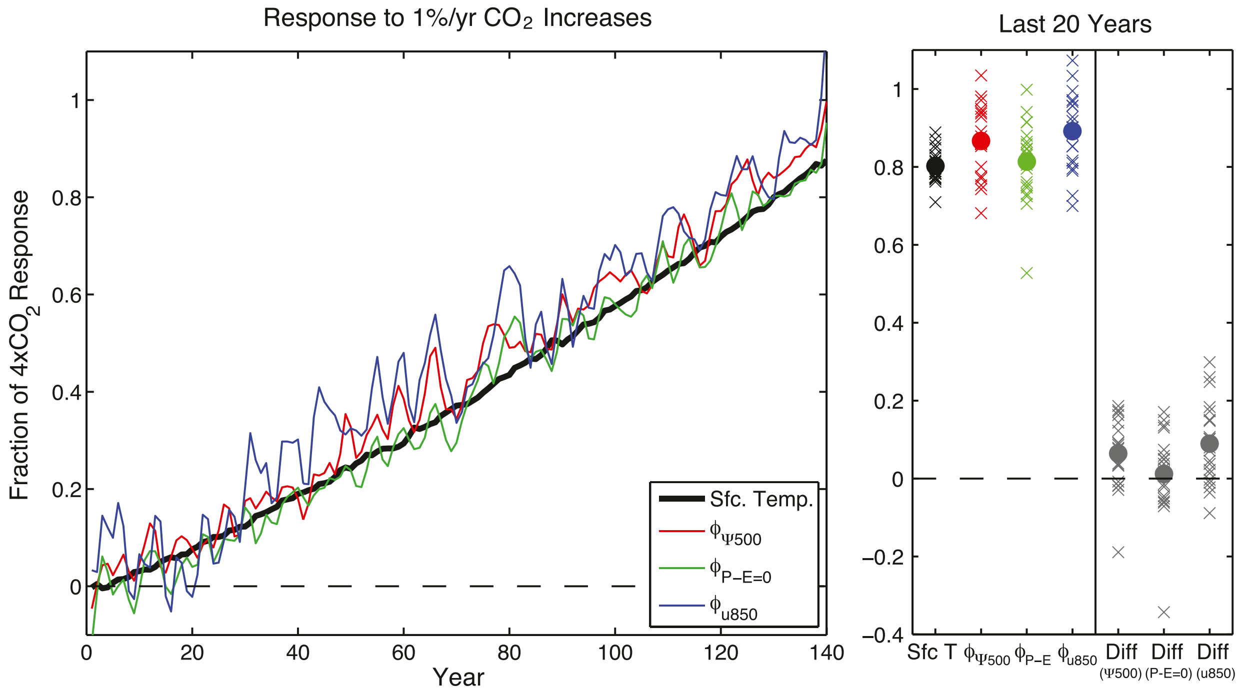

FIG. 10. (left) Time series of the annual-mean, multimodel-mean responses of SH $\phi_{\Psi500}$ (red), $\phi_{P-E=0}$ (green), and ϕ_{u850} (blue) and global-mean surface temperature (black) to 1% yr^{-1} increases in CO_2 from preindustrial levels. The responses are plotted in terms of the fraction of the total response to 4 × CO_2 (defined as the average over years 101–150 shown in the right panel of Fig. 1). The time series have been low-pass filtered for plotting purposes. (right) As in the right panels of Fig. 2, but for the last 20 yr of the 1% yr^{-1} CO_2 scenario.

levels in the troposphere rise with the global-mean surface temperature.

Examining interannual variability in the control runs of CMIP5 models, we find that interannual variability in SH $\phi_{P-E=0}$ is significantly correlated with that of SH $\phi_{\Psi500}$, as noted by previous studies. On average, SH $\phi_{P-E=0}$ shifts poleward by 0.6°–0.7° for every 1° shift in $\phi_{\Psi500}$ (see also Fig. 6 of Polvani et al. 2011), although the exact ratio varies by model (from 0.4:1 to 1:1). This ratio is consistent with the fact that, during the first ~10 yr following abrupt CO_2 quadrupling, the response of SH $\phi_{P-E=0}$ is ~60%–70% of that of $\phi_{\Psi500}$ (cf. green and red lines in Fig. 1). Hence, the SH subtropical dry zone edge does indeed shift poleward consistently with the rapid time-scale expansion of the SH Hadley cell.

However, in contrast to interannual variability when mean circulation changes dominate SH $\phi_{P-E=0}$ variability, when atmospheric CO_2 is increased, SH $\phi_{P-E=0}$ subsequently undergoes an additional poleward shift on the time scale of the global-mean surface temperature rise, consistent with driving by eddy moisture fluxes in a warming climate (Fig. 9, purple line). As a result, by the end of the abrupt 4 × CO_2 scenario, the magnitudes of the multimodel-mean responses of $\phi_{P-E=0}$ and $\phi_{\Psi500}$ are nearly identical (Fig. 1; see also Fig. 2 of Lu et al. 2007) and no longer follow the ~0.7:1.0 ratio found from interannual variability. Again, we note that these ratios reflect the multimodel mean, but in all but one model, the ratio between the poleward shifts in SH $\phi_{P-E=0}$ and $\phi_{\Psi500}$ increases throughout the duration of the abrupt 4 × CO_2 scenario (not shown).

d. *Relevance of results to more realistic CO_2 forcings*

Finally, one may question whether the results in this study are relevant for more realistic future scenarios, in which atmospheric CO_2 concentrations increase progressively over time. To address this issue, in Fig. 10, we have repeated our analysis from Fig. 1 using the 1% yr^{-1} CO_2 increase scenario. Here, as in Fig. 2, we have plotted each of the responses in terms of the fraction of their total response to 4 × CO_2 forcing. At first glance, all three circulation metrics appear to increase monotonically with global-mean surface temperature. However, on closer inspection, one can see that ϕ_{u850} and $\phi_{\Psi500}$ are adjusting to their final values at a slightly faster rate than $\phi_{P-E=0}$ and the global-mean surface temperature, consistent with the results from Fig. 1 (i.e., the blue and red lines are consistently above the green and black lines in Fig. 10). By the last 20 yr of the 1% yr^{-1} CO_2 scenario, ϕ_{u850} and $\phi_{\Psi500}$ have achieved a larger fraction of their total $4 \times CO_2$ response than the global-mean surface temperature in 16 out of 21 models (Fig. 10, right) and $\phi_{P-E=0}$ in 15 out of 21 models (not shown). Hence, there is some limited evidence that, even in slowly increasing CO_2 scenarios, some aspects of the atmospheric circulation appear to equilibrate faster than the global-mean surface temperature. To our knowledge, this has not been noted before in the literature.

4. Conclusions

In this study, we have examined the time scales of the SH tropospheric circulation response to increasing atmospheric CO_2 concentrations. We found that key elements of the circulation response, including the poleward shift of the midlatitude jet and Hadley cell edge, evolve on a faster time scale than the global-mean surface temperature, particularly during the JJA and SON seasons (Figs. 1 and 5). The time scales of the SH tropospheric circulation response appear closely linked to the meridional temperature gradient in the upper troposphere–lower stratosphere and, in particular, to the temperatures in the polar lower stratosphere.

During all seasons, warming global surface temperatures contribute to large warming in the tropical upper troposphere, consistent with the moist adiabatic adjustment of tropical tropospheric lapse rates to surface warming (Figs. 4f and 6a). During DJF and MAM, warming global surface temperatures also contribute to substantial cooling in the SH polar lower stratosphere, consistent with the rising of the tropopause height (Figs. 6b and 8c). Consequently, during DJF and MAM, warming global surface temperatures drive the time scales of the meridional temperature gradient in the upper troposphere–lower stratosphere and thus the SH tropospheric circulation response.

However, during JJA and SON, warming global surface temperatures contribute to very slight warming in the SH polar lower stratosphere (Figs. 6b and 8f), as there is little difference between the climatological polar tropospheric and stratospheric lapse rates during these seasons (Fig. 7b). As a result, the SH polar lower-stratospheric temperature response is dominated by the cooling influence of the direct radiative effects of increased CO_2 (Fig. 8e), and hence SH polar lower-stratospheric temperatures reach their equilibrium levels on a much faster time scale than the global-mean surface temperature during these seasons (Fig. 6b, orange and red lines). Consequently, during JJA and SON, the fast time-scale effects of the direct radiative forcing of CO_2 have a stronger influence on the meridional temperature gradient in the upper troposphere–lower stratosphere and thus on the SH tropospheric circulation response (see also Table 3).

Gerber and Son (2014) previously identified polar lower-stratospheric cooling as a key factor in driving the tropospheric circulation response to stratospheric ozone depletion, and we show here that it is also a key factor in understanding the tropospheric circulation response to increasing greenhouse gas concentrations (Table 2; see also Fig. 11 of Lorenz and DeWeaver 2007). Our paper adds to the emerging evidence that the rapid adjustment of stratospheric temperatures to the radiative forcing of CO_2 may affect the tropospheric circulation on much faster time scales than that expected from rising global-mean surface temperatures (Wu et al. 2013a; Staten et al. 2014). Furthermore, our paper highlights how other elements of the SH tropospheric circulation response, notably the poleward shift in the subtropical dry zones, are supplemented by eddy moisture fluxes and hence evolve on slower time scales that are more in line with that of the global-mean surface temperature (Fig. 9). Consequently, some circulation metrics may be more appropriate than others in detecting emerging anthropogenic influences in the atmospheric general circulation.

Acknowledgments. We thank Isaac Held, Karen Shell, Geoff Vallis, Darryn Waugh, and two anonymous reviewers for helpful comments. All data used in this paper are freely available through the Earth System Grid Federation (https://pcmdi.llnl.gov/search/cmip5/) as described in Taylor et al. (2012). We acknowledge the WCRP's Working Group on Coupled Modelling, which is responsible for CMIP, and we thank the climate modeling groups (listed in Table 1) for producing and making available their model output. For CMIP, the U.S. Department of Energy's PCMDI provides coordinating support and led development of software infrastructure in partnership with the Global Organization for Earth System Science Portals. This material is based upon work supported by the National Science Foundation under Grant AGS-1522829. L.M.P. is also supported by a NSF grant to Columbia University.

APPENDIX

Understanding the Intermodel Spread in the Wintertime SH ϕ_{u850} Response to $4 \times CO_2$ Forcing

In Table 2, we show that the intermodel spread in the SH ϕ_{u850} response to $4 \times CO_2$ forcing is significantly correlated with the polar lower-stratospheric temperature response during all seasons. In section 3b, we

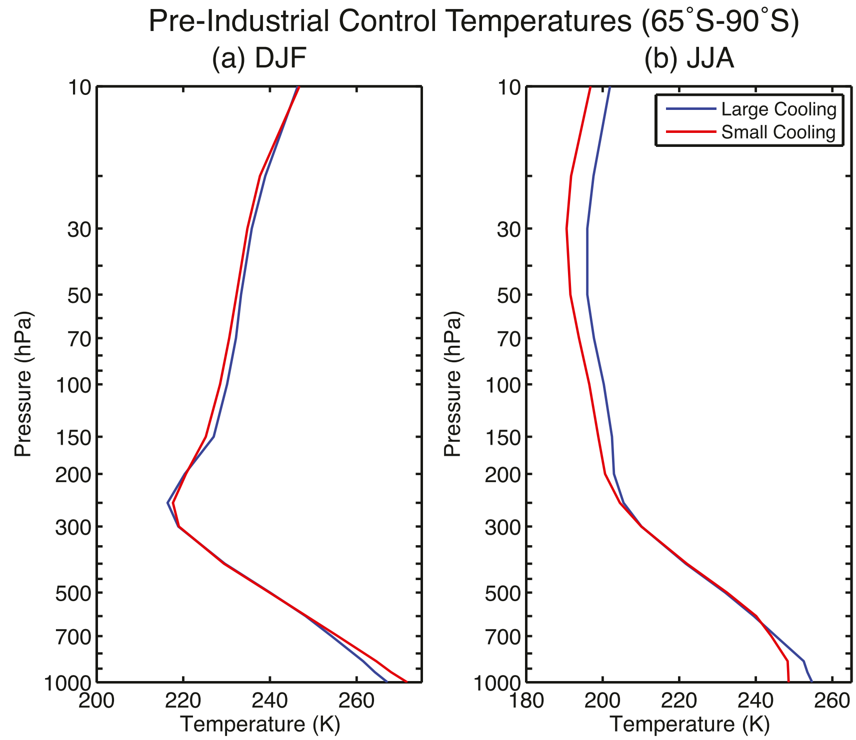

FIG. A1. As in Figs. 7a and 7b, but for preindustrial control temperature profiles averaged over the 10 CMIP5 models examined in this study with the largest polar lower-stratospheric (150–200 hPa; 65°–90°S) cooling responses to 4 × CO_2 forcing (blue) (after years 101–150 of the abrupt 4 × CO_2 run) and the 10 CMIP5 models with the smallest polar lower-stratospheric cooling responses (red). The subsets are defined separately for each season.

explain that the correlations between the SH ϕ_{u850} response and polar lower-stratospheric temperature response during DJF and MAM can be expected from the intermodel spread in equilibrium climate sensitivity. In this appendix, we explain that the correlations between the SH ϕ_{u850} response and polar lower-stratospheric temperature response during JJA and SON can be expected from the intermodel spread in the control climatologies of the models.

To demonstrate this, Fig. A1 shows the composites of the preindustrial control temperature profiles averaged over SH high latitudes for two subsets of CMIP5 models: 1) the 10 models with the largest polar lower-stratospheric (150–200 hPa; 65°–90°S) cooling responses to 4 × CO_2 forcing (plotted in blue) and 2) the 10 models with the smallest polar lower-stratospheric cooling responses to 4 × CO_2 forcing (plotted in red). These subsets are defined separately for each season. There is little difference in the climatological temperature profiles between the two subsets of models in DJF (Fig. A1a), but in JJA, the models that cool more strongly in response to 4 × CO_2 forcing (Fig. A1b, blue) have warmer climatological temperatures in the polar stratosphere. This result is unlikely to occur by chance. If we randomly select two subsets of 10 models, the difference in climatological polar stratospheric temperatures seen in Fig. A1b only occurs in ~0.5% of random selections (based on a Monte Carlo test of 1000 random selections).

The key difference between the two subsets of models in Fig. A1b arises from the lapse rate of the temperature profile near the tropopause (note the kink in the blue line immediately above 250 hPa and the absence of a kink in the red line): models with the largest climatological lapse rates in the wintertime stratosphere (as measured by the temperature difference over the 70–250-hPa layer) have the smallest cooling responses in the polar lower stratosphere in response to 4 × CO_2 forcing (r = 0.78 for JJA and r = 0.64 for SON). As discussed by Vallis et al. (2015), if the tropopause temperature remains fixed, the climatological lapse rate is important for understanding the effects of an increase in tropopause height on stratospheric temperatures (see their Fig. 11). When the lapse rate changes sign at the tropopause (such as during the DJF season; Fig. 7a), an increase in the tropopause height will result in cooling at lower-stratospheric levels (see also Fig. 8c). However, the more positive the lapse rate becomes above the tropopause (i.e., the less temperatures increase with height or the more temperatures decrease with height), the less important this effect becomes (e.g., cf. DJF and JJA seasons in Figs. 7 and 8). Hence, all else being equal, models with the most positive climatological lapse rates above the tropopause (i.e., with the largest temperatures decreases with height; Fig. A1b, red) might be expected to have the smallest cooling responses in the polar lower stratosphere, in agreement with the results shown in Fig. A1b.

The results in Table 2 reveal that the poleward shift in SH ϕ_{u850} in response to $4 \times CO_2$ forcing is closely linked to the polar lower-stratospheric temperature response, and the results in Fig. A1 reveal that the polar lower-stratospheric temperature response is closely linked to the preindustrial control temperature profile during winter months. Therefore, poleward shifts in SH ϕ_{u850} in response to $4 \times CO_2$ forcing are significantly correlated with the preindustrial control climatological lapse rates in the polar lower stratosphere (65°–90°S, 70–250 hPa) during the JJA ($r = -0.56$) and SON ($r = -0.61$) seasons; that is, the models with the largest poleward jet shifts during winter months have climatological polar stratospheric temperatures that decrease the least with height above the tropopause. This result is in agreement with the relationship between the models' wintertime control climatologies and SH ϕ_{u850} responses documented in previous studies (e.g., Grise and Polvani 2014b; Simpson and Polvani 2016).

REFERENCES

Allen, M. R., and W. J. Ingram, 2002: Constraints on future changes in the hydrological cycle. *Nature*, **419**, 224–228, doi:10.1038/nature01092.

Arblaster, J. M., G. A. Meehl, and D. J. Karoly, 2011: Future climate change in the Southern Hemisphere: Competing effects of ozone and greenhouse gases. *Geophys. Res. Lett.*, **38**, L02701, doi:10.1029/2010GL045384.

Barnes, E. A., and L. M. Polvani, 2013: Response of the midlatitude jets and of their variability to increased greenhouse gases in CMIP5 models. *J. Climate*, **26**, 7117–7135, doi:10.1175/JCLI-D-12-00536.1.

Bony, S., G. Bellon, D. Klocke, S. Sherwood, S. Fermepin, and S. Denvil, 2013: Robust direct effect of carbon dioxide on tropical circulation and regional precipitation. *Nat. Geosci.*, **6**, 447–451, doi:10.1038/ngeo1799.

Brayshaw, D. J., B. Hoskins, and M. Blackburn, 2008: The storm-track response to idealized SST perturbations in an aquaplanet GCM. *J. Atmos. Sci.*, **65**, 2842–2860, doi:10.1175/2008JAS2657.1.

Butler, A. H., D. W. J. Thompson, and R. Heikes, 2010: The steady-state atmospheric circulation response to climate change–like thermal forcings in a simple general circulation model. *J. Climate*, **23**, 3474–3496, doi:10.1175/2010JCLI3228.1.

Chen, G., R. A. Plumb, and J. Lu, 2010: Sensitivities of zonal mean atmospheric circulation to SST warming in an aqua-planet model. *Geophys. Res. Lett.*, **37**, L12701, doi:10.1029/2010GL043473.

Collins, M., and Coauthors, 2014: Long-term climate change: Projections, commitments, and irreversibility. *Climate Change 2013: The Physical Science Basis*, T. F. Stocker et al., Eds., Cambridge University Press, 1029–1136.

Deser, C., and A. S. Phillips, 2009: Atmospheric circulation trends, 1950–2000: The relative roles of sea surface temperature forcing and direct atmospheric radiative forcing. *J. Climate*, **22**, 396–413, doi:10.1175/2008JCLI2453.1.

Forster, P. M., T. Andrews, P. Good, J. M. Gregory, L. S. Jackson, and M. Zelinka, 2013: Evaluating adjusted forcing and model spread for historical and future scenarios in the CMIP5 generation of climate models. *J. Geophys. Res. Atmos.*, **118**, 1139–1150, doi:10.1002/jgrd.50174.

Frierson, D. M. W., J. Lu, and G. Chen, 2007: Width of the Hadley cell in simple and comprehensive general circulation models. *Geophys. Res. Lett.*, **34**, L18804, doi:10.1029/2007GL031115.

Garfinkel, C. I., D. W. Waugh, and E. P. Gerber, 2013: The effect of tropospheric jet latitude on coupling between the stratospheric polar vortex and the troposphere. *J. Climate*, **26**, 2077–2095, doi:10.1175/JCLI-D-12-00301.1.

Gerber, E. P., and S.-W. Son, 2014: Quantifying the summertime response of the austral jet stream and Hadley cell to stratospheric ozone and greenhouse gases. *J. Climate*, **27**, 5538–5559, doi:10.1175/JCLI-D-13-00539.1.

Grise, K. M., and L. M. Polvani, 2014a: The response of midlatitude jets to increased CO_2: Distinguishing the roles of sea surface temperature and direct radiative forcing. *Geophys. Res. Lett.*, **41**, 6863–6871, doi:10.1002/2014GL061638.

——, and ——, 2014b: Is climate sensitivity related to dynamical sensitivity? A Southern Hemisphere perspective. *Geophys. Res. Lett.*, **41**, 534–540, doi:10.1002/2013GL058466.

——, and ——, 2016: Is climate sensitivity related to dynamical sensitivity? *J. Geophys. Res. Atmos.*, **121**, 5159–5176, doi:10.1002/2015JD024687.

Harvey, B. J., L. C. Shaffrey, and T. J. Woollings, 2014: Equator-to-pole temperature differences and the extra-tropical storm track responses of the CMIP5 climate models. *Climate Dyn.*, **43**, 1171–1182, doi:10.1007/s00382-013-1883-9.

He, J., and B. J. Soden, 2015: Anthropogenic weakening of the tropical circulation: The relative roles of direct CO_2 forcing and sea surface temperature change. *J. Climate*, **28**, 8728–8742, doi:10.1175/JCLI-D-15-0205.1.

——, and ——, 2017: A re-examination of the projected subtropical precipitation decline. *Nat. Climate Change*, **7**, 53–57, doi:10.1038/nclimate3157.

Held, I. M., and B. J. Soden, 2006: Robust responses of the hydrological cycle to global warming. *J. Climate*, **19**, 5686–5699, doi:10.1175/JCLI3990.1.

Ivy, D. J., C. Hilgenbrink, D. Kinnison, R. Alan Plumb, A. Sheshadri, S. Solomon, and D. J. Thompson, 2017: Observed changes in the Southern Hemispheric circulation in May. *J. Climate*, **30**, 527–536, doi:10.1175/JCLI-D-16-0394.1.

Johanson, C. M., and Q. Fu, 2009: Hadley cell widening: Model simulations versus observations. *J. Climate*, **22**, 2713–2725, doi:10.1175/2008JCLI2620.1.

Kang, S. M., and L. M. Polvani, 2011: The interannual relationship between the latitude of the eddy-driven jet and the edge of the Hadley cell. *J. Climate*, **24**, 563–568, doi:10.1175/2010JCLI4077.1.

——, and J. Lu, 2012: Expansion of the Hadley cell under global warming: Winter versus summer. *J. Climate*, **25**, 8387–8393, doi:10.1175/JCLI-D-12-00323.1.

Kushner, P. J., I. M. Held, and T. L. Delworth, 2001: Southern Hemisphere atmospheric circulation response to global warming. *J. Climate*, **14**, 2238–2249, doi:10.1175/1520-0442(2001)014<0001:SHACRT>2.0.CO;2.

Lorenz, D. J., and E. T. DeWeaver, 2007: Tropopause height and zonal wind response to global warming in the IPCC scenario integrations. *J. Geophys. Res.*, **112**, D10119, doi:10.1029/2006JD008087.

Lu, J., G. A. Vecchi, and T. Reichler, 2007: Expansion of the Hadley cell under global warming. *Geophys. Res. Lett.*, **34**, L06805, doi:10.1029/2006GL028443.

——, G. Chen, and D. M. W. Frierson, 2010: The position of the midlatitude storm track and eddy-driven westerlies in aquaplanet ACGMs. *J. Atmos. Sci.*, **67**, 3984–4000, doi:10.1175/2010JAS3477.1.

Merlis, T., 2015: Direct weakening of tropical circulations from masked CO_2 radiative forcing. *Proc. Natl. Acad. Sci. USA*, **112**, 13 167–13 171, doi:10.1073/pnas.1508268112.

Polvani, L. M., and P. J. Kushner, 2002: Tropospheric response to stratospheric perturbations in a relatively simple general circulation model. *Geophys. Res. Lett.*, **29**, 1114, doi:10.1029/2001GL014284.

——, D. W. Waugh, G. J. P. Correa, and S.-W. Son, 2011: Stratospheric ozone depletion: The main driver of twentieth-century atmospheric circulation changes in the Southern Hemisphere. *J. Climate*, **24**, 795–812, doi:10.1175/2010JCLI3772.1.

Quan, X.-W., M. P. Hoerling, J. Perlwitz, H. F. Diaz, and T. Xu, 2014: How fast are the tropics expanding? *J. Climate*, **27**, 1999–2013, doi:10.1175/JCLI-D-13-00287.1.

Reichler, T., M. Dameris, and R. Sausen, 2003: Determining the tropopause height from gridded data. *Geophys. Res. Lett.*, **30**, 2042, doi:10.1029/2003GL018240.

Ring, M. J., and R. A. Plumb, 2008: The response of a simplified GCM to axisymmetric forcings: Applicability of the fluctuation–dissipation theorem. *J. Atmos. Sci.*, **65**, 3880–3898, doi:10.1175/2008JAS2773.1.

Scheff, J., and D. M. W. Frierson, 2012: Robust future precipitation declines in CMIP5 largely reflect the poleward expansion of model subtropical dry zones. *Geophys. Res. Lett.*, **39**, L18704, doi:10.1029/2012GL052910.

Seager, R., and N. Naik, 2012: A mechanisms-based approach to detecting recent anthropogenic hydroclimate change. *J. Climate*, **25**, 236–261, doi:10.1175/JCLI-D-11-00056.1.

——, ——, and G. A. Vecchi, 2010: Thermodynamic and dynamic mechanisms for large-scale changes in the hydrological cycle in response to global warming. *J. Climate*, **23**, 4651–4668, doi:10.1175/2010JCLI3655.1.

Shaw, T. A., and A. Voigt, 2015: Tug of war on summertime circulation between radiative forcing and sea surface warming. *Nat. Geosci.*, **8**, 560–566, doi:10.1038/ngeo2449.

Simpson, I., and L. M. Polvani, 2016: Revisiting the relationship between jet position, forced response and annular mode variability in the southern mid-latitudes. *Geophys. Res. Lett.*, **43**, 2896–2903, doi:10.1002/2016GL067989.

——, T. Shaw, and R. Seager, 2014: A diagnosis of the seasonally and longitudinally varying midlatitude circulation response to global warming. *J. Atmos. Sci.*, **71**, 2489–2515, doi:10.1175/JAS-D-13-0325.1.

Solomon, A., L. M. Polvani, D. W. Waugh, and S. Davis, 2016: Contrasting upper and lower atmospheric metrics of tropical expansion in the Southern Hemisphere. *Geophys. Res. Lett.*, **43**, 10 496–10 503, doi:10.1002/2016GL070917.

Staten, P. W., J. J. Rutz, T. Reichler, and J. Lu, 2012: Breaking down the tropospheric circulation response by forcing. *Climate Dyn.*, **39**, 2361–2375, doi:10.1007/s00382-011-1267-y.

——, T. Reichler, and J. Lu, 2014: The transient circulation response to radiative forcings and sea surface warming. *J. Climate*, **27**, 9323–9336, doi:10.1175/JCLI-D-14-00035.1.

Stephenson, D. B., and I. M. Held, 1993: GCM response of northern winter stationary waves and storm tracks to increasing amounts of carbon dioxide. *J. Climate*, **6**, 1859–1870, doi:10.1175/1520-0442(1993)006<1859:GRONWS>2.0.CO;2.

Taylor, K. E., R. J. Stouffer, and G. A. Meehl, 2012: An overview of CMIP5 and the experiment design. *Bull. Amer. Meteor. Soc.*, **93**, 485–498, doi:10.1175/BAMS-D-11-00094.1.

Thompson, D. W. J., and J. M. Wallace, 2000: Annular modes in the extratropical circulation. Part I: Month-to-month variability. *J. Climate*, **13**, 1000–1016, doi:10.1175/1520-0442(2000)013<1000:AMITEC>2.0.CO;2.

——, and S. Solomon, 2002: Interpretation of recent Southern Hemisphere climate change. *Science*, **296**, 895–899, doi:10.1126/science.1069270.

——, M. P. Baldwin, and S. Solomon, 2005: Stratosphere–troposphere coupling in the Southern Hemisphere. *J. Atmos. Sci.*, **62**, 708–715, doi:10.1175/JAS-3321.1.

——, S. Solomon, P. J. Kushner, M. H. England, K. M. Grise, and D. J. Karoly, 2011: Signatures of the Antarctic ozone hole in Southern Hemisphere surface climate change. *Nat. Geosci.*, **4**, 741–749, doi:10.1038/ngeo1296.

Vallis, G. K., P. Zurita-Gotor, C. Cairns, and J. Kidston, 2015: Response of the large-scale structure of the atmosphere to global warming. *Quart. J. Roy. Meteor. Soc.*, **141**, 1479–1501, doi:10.1002/qj.2456.

Wang, S., E. P. Gerber, and L. M. Polvani, 2012: Abrupt circulation responses to tropical upper tropospheric warming in a relatively simple stratosphere-resolving AGCM. *J. Climate*, **25**, 4097–4115, doi:10.1175/JCLI-D-11-00166.1.

Wilcox, L. J., A. J. Charlton-Perez, and L. J. Gray, 2012: Trends in austral jet position in ensembles of high- and low-top CMIP5 models. *J. Geophys. Res.*, **117**, D13115, doi:10.1029/2012JD017597.

Williams, G. P., 2006: Circulation sensitivity to tropopause height. *J. Atmos. Sci.*, **63**, 1954–1961, doi:10.1175/JAS3762.1.

Wu, Y., R. Seager, M. Ting, N. H. Naik, and T. A. Shaw, 2012: Atmospheric circulation response to an instantaneous doubling of carbon dioxide. Part I: Model experiments and transient thermal response in the troposphere. *J. Climate*, **25**, 2862–2879, doi:10.1175/JCLI-D-11-00284.1.

——, ——, T. A. Shaw, M. Ting, and N. Naik, 2013a: Atmospheric circulation response to an instantaneous doubling of carbon dioxide. Part II: Atmospheric transient adjustment and its dynamics. *J. Climate*, **26**, 918–935, doi:10.1175/JCLI-D-12-00104.1.

——, L. M. Polvani, and R. Seager, 2013b: The importance of the Montreal Protocol in protecting the Earth's hydroclimate. *J. Climate*, **26**, 4049–4067, doi:10.1175/JCLI-D-12-00675.1.